Journal of The Electrochemical Society, **156** (12) B1417-B1422 (2009)
0013-4651/2009/156(12)/B1417/6/$25.00 © The Electrochemical Society

Diffusion Impedance on Nickel/Gadolinia-Doped Ceria Anodes for Solid Oxide Fuel Cells

P. V. Aravind,[a,z] J. P. Ouweltjes,[b] and J. Schoonman[c]

[a]*Section Energy Technology, Delft University of Technology, 2628 CA Delft, The Netherlands*
[b]*Energy Research Center of the Netherlands, 1755 LE Petten, The Netherlands*
[c]*Laboratory for Inorganic Chemistry, Delft University of Technology, 2628 BL Delft, The Netherlands*

Electrochemical impedance measurements were carried out on symmetrical nickel/gadolinia-doped ceria test cells. For H_2, N_2, and H_2O mixtures, the diffusion length obtained based on the impedance measurements is on the order of centimeters. This high value of the diffusion length is attributed to the flow field in the reactor. It is suggested that a detailed analysis of the gas flow field inside the test reactor is essential before interpreting the impedance measurements with various solid oxide fuel cell test configurations.
 [DOI: 10.1149/1.3231490]

Manuscript submitted May 7, 2009; revised manuscript received August 17, 2009. Published October 9, 2009; publisher error corrected October 23, 2009.

Electrochemical impedance spectroscopy (EIS) for evaluating the performance of solid oxide fuel cell (SOFC) anodes with different fuels with and without contaminants has been reported before.[1-9] The objective of the work reported in this paper is to evaluate the impedance spectra recorded on symmetrical test cells with nickel/gadolinia-doped ceria (Ni/GDC) electrodes to understand the influence of gas-phase processes on electrode performance. It is intended that once the arcs due to gas-phase processes in the spectra are identified, the rest of the spectra can be analyzed to study the influence of fuel gas composition or contaminants present in it on the electrode. Studies on gas-phase processes at SOFC anodes have been reported.[1,6,10-13] Primdahl and Mogensen studied gas-phase processes with complete cells having reference electrodes mounted in a two-gas atmosphere and symmetrical test cells kept under a single gas atmosphere. For an anode of a test cell consisting of a working electrode, a counter electrode, and a reference electrode, an arc that appeared in the low frequency part of the spectra was ascribed to gas conversion.[6] It was also proposed that an arc that appeared at the medium frequency part of the spectra (10–100 Hz) was due to gas diffusion limitations. Gas conversion impedance was not reported with the measurements on symmetrical cells under a single gas atmosphere. Bessler developed a numerical model for the impedance due to combined gas-flow limitations (diffusion, convection, etc.) for a similar gas-flow scheme as used by Primdahl (for an anode as part of a complete cell with a reference electrode) and he concluded that in such a setup, the diffusion, convection, etc., have a combined effect and have to be treated together.[10] Bessler proposed the name "gas concentration impedance" to describe the impedance due to transport processes in the gas phase and suggested using the name "gas diffusion impedance" when the mass transport is only due to diffusion.

Gewies et al. used Ni/yttria-stabilized zirconia (YSZ) symmetrical electrodes and Aravind used Ni/GDC symmetrical electrodes to carry out EIS measurements under a single gas atmosphere.[1,9] The observation of an arc at the low frequencies due to diffusion limitations was reported in both cases. Aravind, with a simple diffusion resistance model, and Gewies et al., with detailed kinetic modeling, showed rather high diffusion lengths on the order of centimeters. This paper presents the results from the diffusion resistance measurements on Ni/GDC electrodes.

Experimental

The focus of this paper is on the analysis of the EIS spectra for symmetrical anode samples in a test setup with a single gas chamber and with various inlet fuel gas compositions. The test setup employed was developed at the Energy research Center of the Netherlands (ECN). The gas-flow configuration for the test cell is presented schematically in Fig. 1.

[z] E-mail: p.v.aravind@tudelft.nl

The prepared Ni/GDC electrodes consisted of the following three layers: (*i*) a layer of $Gd_{0.4}Ce_{0.6}O_{1.8}$ + 2 mol % CoO (which gets converted to metallic cobalt under reducing conditions) adjacent to the electrolyte for better adherence between the electrolyte and the functional layer, (*ii*) a functional layer of $NiO/Gd_{0.1}Ce_{0.9}O_{1.95}$ 65/35 wt %, and (*iii*) a contact layer of NiO. The anodes were 22 mm in diameter and were screen-printed to 130–140 μm thick 3YSZ electrolytes 25 mm in diameter and sintered at 1473 K in air. The contact layer was approximately 3–5 μm thick, the functional layer was approximately 25–30 μm thick, and the nickel layer was around 5 μm thick.

The test cells were clamped between ceramic supports. These supports were 5 mm thick. Each of these supports had two layers, with each layer having several parallel channels of 1 mm width and 2.5 mm depth. The channels in these two layers were perpendicular to each other so that the gas was easily distributed (Fig. 1b). The top support covered the complete area of the test cell and the bottom support had a circular opening 4 mm in diameter at the center to keep a thermocouple close to the sample. Thin gold meshes were used on either side of the test cell for current collection. The sample and the ceramic supports were kept horizontal on a ceramic platform supported by a ceramic rod. An additional ceramic weight was kept on the top of the upper ceramic support. The sample was kept in a single-gas chamber through which the fuel gas was passed. The sample support and the gas chamber were kept vertical, with the gas flowing upward. Gas-flow patterns inside the test setup are shown in Appendix B.

Before the testing, the samples were heated in a nitrogen stream. Reduction of the anode sample was performed at 1123 K. Initially, a nitrogen stream of 0.1 N L/min with a moisture level of 2.5% by

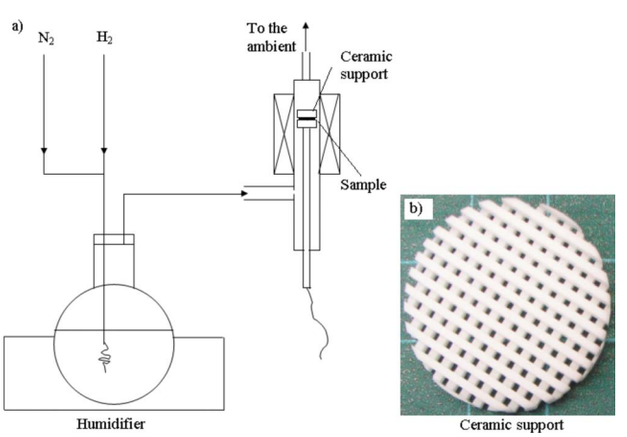

Figure 1. (Color online) (a) The experimental setup. (b) The ceramic support.

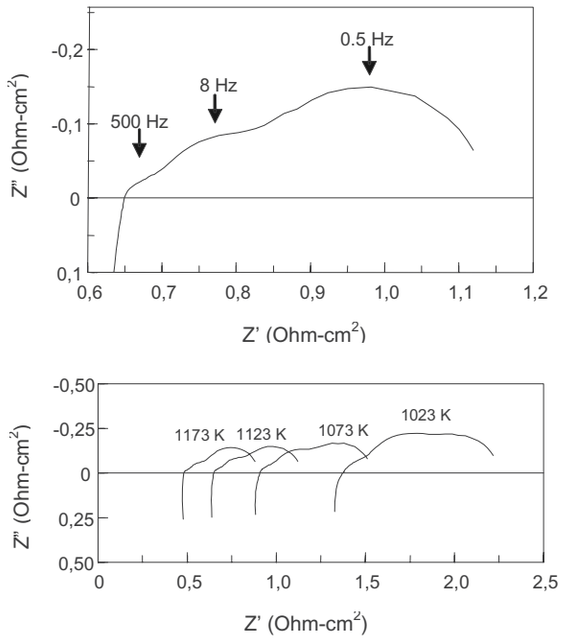

Figure 2. Impedance spectra obtained with humidified hydrogen at 1123 K (top) and at different temperatures (bottom).

volume was used to flush the sample for 5 min. The nitrogen flow was then replaced stepwise by humidified hydrogen, with 5 min steps of hydrogen flow of 0.005, 0.02, and finally 0.1 N L/min (the flow rate of dry hydrogen is given). Following a stabilization period of approximately 1 h, impedance spectra were recorded for 12 h with a period of 2 h in between to confirm that the reduction of the sample had taken place.

EIS measurements were performed with a Solartron 1255 frequency response analyzer in combination with a Solartron 1287 electrochemical interface. The measurements on the samples were taken at zero bias in the frequency range between 0.1 Hz and 100 kHz with a signal amplitude of 10 mV.

The experiments were started with humidified hydrogen. The hydrogen feed was subsequently diluted in steps by adding 15 mL/min nitrogen at each step until a composition of 40 mL/min H_2 and 60 mL/min N_2 was obtained. The fuel was humidified at a temperature of 303 K. Experiments were carried out at four different temperatures: 1023, 1073, 1123, and 1173 K. Additional measurements were carried out at 1123 K with two more humidity levels (with moist hydrogen stream), with humidification temperatures at 306 and 309 K.

Results and Discussion

The experiments with moist hydrogen were carried out at various temperatures. It was observed that the spectra comprised mainly three arcs. For the spectra at 1123 K, the following characteristics were observed. The first arc at the highest frequency had a peak at around 500 Hz, the one at medium frequencies had a peak at around 8 Hz, and the lowest frequency arc revealed a peak at around 0.5 Hz. It was also observed that the total impedance increases at lower temperatures with the same inlet gas composition as shown in Fig. 2.

The recorded data were analyzed in the following way. It is assumed that impedance spectra can be interpreted using an electrical equivalent circuit, describing a number of independent rate-limiting processes in series/parallel arrangements. Three different arcs observed were ascribed to three different processes. The arc observed at high frequencies is considered as representing process 1. Similarly, the arc at medium frequencies is considered as representing process 2 and the arc at low frequencies is considered as representing process 3. The obtained impedance spectra were fitted with the following elements using the software Z-View. For processes 1 and 2, the equivalent subcircuit (RQ) with a resistance R and a constant-phase element Q in parallel was applied. The admittance of Q is $Y^* = Y_0(j\omega)^n$, where Y_0 is an adjustable admittance depending on the characteristics of the corresponding process, j is the imaginary unit, ω is the angular frequency, and n is a frequency exponent.[6] When n is consistently unity, Q represents a perfect capacitance. This was the case for process 2. For process 3, diffusion limitation where perfect one-dimensional diffusion in a stagnant layer of a homogeneous gas mixture of finite thickness is assumed and the finite-length Warburg diffusion (with a notation Ws as represented in Z-View) was used. The admittance of the finite-length Warburg diffusion is $Y^* = Y_0\sqrt{j\omega}\coth(T\sqrt{j\omega})$ with an admittance parameter $Y_0 \propto \sqrt{D_{\text{eff}}}$, where D_{eff} is the effective diffusion coefficient of the diffusing reactant in the given gas mixture. The parameter T is given as $T = l/\sqrt{D_{\text{eff}}}$, where l is the thickness of the stagnant gas layer. The diffusion resistance is given by $R_D = T/Y_0$ and is represented by WR in the following analysis.

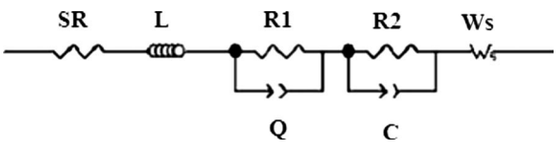

Figure 3. The electrical equivalent circuit used for fitting.

In principle, the n-value should remain constant for a given physical or chemical process. The time constant or the inverse relaxation frequency f_s of the related subcircuit also shall be employed to follow the processes. The relaxation frequency of an RQ subcircuit is given by Eq. 1, and the relaxation frequency for the finite-length Warburg diffusion element by series expansion is given approximately by Eq. 2.[6,14] Identical rate-limiting steps are assumed to occur on both electrodes, and hence the obtained resistances are assumed to be the sum of the corresponding values on each of the electrodes taken separately

$$f_s = \frac{1}{2\pi\sqrt[n]{RY_0}} \quad [1]$$

$$f_s \approx \frac{2.53D_{\text{eff}}}{2\pi l^2} \quad [2]$$

The impedance spectra were fitted to an SR-L-R1Qp-R2Cp-Ws equivalent circuit as shown in Fig. 3. SR is a series resistance, which is expected to be the sum of various resistances such as the electrolyte and contact resistances. This resistance is not expected to contribute to the electrode polarization. L is considered as an inductance associated with the measuring system and is ignored in the present analysis. R1 and R2 represent different circuit elements as given above, and the diffusion resistance WR is obtained from the fit parameters for the circuit element Ws. Total anodic polarization is considered as the sum of R1, R2, and WR. It is considered that the achievement of a good fit of data to the model ensures that the Kramers–Kronig relations are held and this indicates that the system reaches steady-state conditions. Table I summarizes the important observations as obtained from the spectra measured at 1123 K.

Arrhenius plots for various circuit elements from the observed impedance spectra are given in Fig. 4. Activation energies of the various components were calculated and are given in Table II.

Variations in the different R values with temperature at different dilution levels, as obtained from the experiments with dilution of hydrogen by addition of nitrogen, are given in Fig. 5.

The low frequency arc does not vary significantly with temperature and has low activation energy (Fig. 4 and Table II), while the

Table I. Details of various circuit elements obtained after fitting the data for humidified hydrogen at 1123 K.

	Peak freq. (Hz)	Fitted circuit	R (Ω cm^2)	n	Possible cause
Arc 1	500	RQp	0.1613	0.44	Processes within or at the surface of the electrode
Arc 2	8	RCp	0.0499	1	Processes within or on the surface of the electrode
Arc 3	0.5	Ws	0.2304		Gas-phase diffusion

other two arcs are influenced by temperature variations and have rather high activation energy. As the gas diffusion resistance is not expected to be significantly influenced by the temperature, the low frequency arc is further analyzed to evaluate the influence of gas diffusion limitations on it. No detailed analysis of the other arcs is presented here. Primdahl suggested the following equation (Eq. 3) as a convenient form of the well-known gas diffusion resistance for

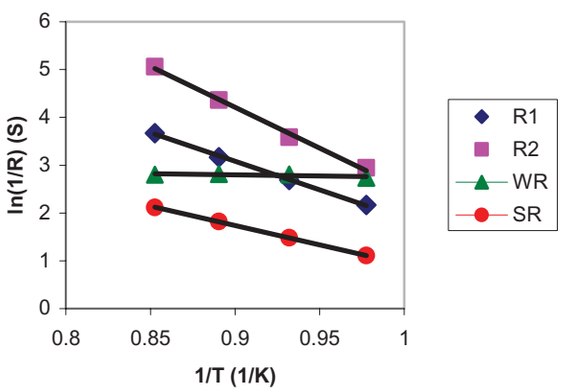

Figure 4. (Color online) Arrhenius plots for different circuit elements. SR stands for the series resistance, R1 stands for the resistance from the first arc, R2 stands for the resistance from the second arc, and WR stands for the resistance of the Warburg element.

Table II. Activation energies for different circuit elements.

Resistance	Activation energy (kJ/mol)
R1	99
R2	142
WR	4

calculating the dc diffusion resistance for an anode of a complete cell with hydrogen fed to the anode chamber and a reference electrode placed in a reference gas.[6] Here, it is assumed that, adjacent to the anode layer, a stagnant gas layer of a thickness on the order of 1 mm is formed and the molecular transport across this layer is mainly due to diffusion. Previously, such an approach has been reported for SOFC cathode flows, too[6]

$$R_d = \eta_D/I = \left(\frac{RT}{2F}\right)^2 \frac{l}{PD_{eff}}\left(\frac{1}{X_{H_2O,B}} + \frac{1}{X_{H_2,B}}\right) \quad [3]$$

Here, R_d is the diffusion resistance, R is the gas constant, η_D is the diffusion overpotential, I is the current, P is the total pressure, D_{eff} is the effective binary diffusion coefficient for H_2–H_2O mixtures, F is the Faraday constant, T is the temperature in kelvin, and $X_{j,B}$ denotes molar fractions of species j in the bulk gas. It is clear from this equation that diffusion limitation is expected to be significant at low reactant concentrations. The given formula is for a single electrode. For the present case, i.e., the symmetric cells, calculated values need to be multiplied by 2.

The developed model holds well for humidified hydrogen at different humidity levels. However, this equation cannot be applied to multicomponent gas mixtures because diffusion coefficients would be different for each of the species in such mixtures and hence an effective binary diffusion coefficient cannot be used. The addition of nitrogen to hydrogen, without varying the moisture level in the gas mix, appeared to increase the diffusion impedance significantly as presented in Fig. 6. This is not well explained by Eq. 3. Based on the Stefan–Maxwell approach for multicomponent gas diffusion and considering the symmetrical cells, the following equation (Eq. 4) is suggested for calculating the diffusion resistance R_d (details are given in Appendix A)[15]

$$R_d = \eta_D/I = 2\left(\frac{RT}{2F}\right)^2 \frac{l}{P}\left(\frac{1}{D_{H_2O-mix}X_{H_2O,B}} + \frac{1}{D_{H_2-mix}X_{H_2,B}}\right) \quad [4]$$

where D_{H_2-mix} and D_{H_2O-mix} are the Stefan–Maxwell diffusion coefficients for hydrogen and water molecules in the given gas flows.

To verify that the low frequency arc of the impedance spectra represents gas-phase diffusion, a detailed analysis is presented here. Using Eq. 4, gas diffusion resistance values were calculated for various gas mixtures employed at the temperatures at which the measurements were taken. These calculated values were compared with the measured values. The following assumption was made. The diffusion length is 1.92 cm, so that the calculated values agree with the whole range of measured values. Root-mean-square error (RMSE) values were calculated to check the variation between calculated and measured values. The diffusion length proposed here is significantly higher than the diffusion length considered by Primdahl and Mogensen. Figure 6 presents the measured diffusion resistance

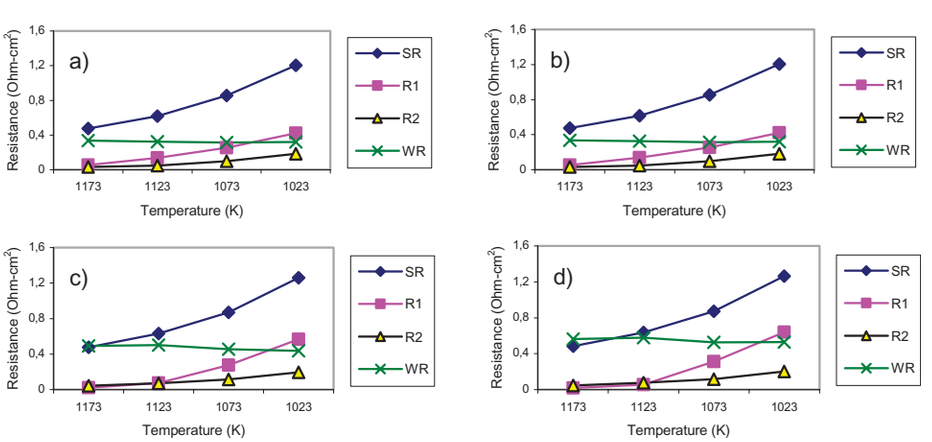

Figure 5. (Color online) Variation of the different measured R values with addition of nitrogen to the hydrogen flow. Dry mixtures are always kept at 100 mL/min and then humidified to 4.2%. (a) 15% N_2, (b) 30% N_2, (c) 45% N_2, and (d) 60% N_2. (Nitrogen percentage is given for the dry mixture.)

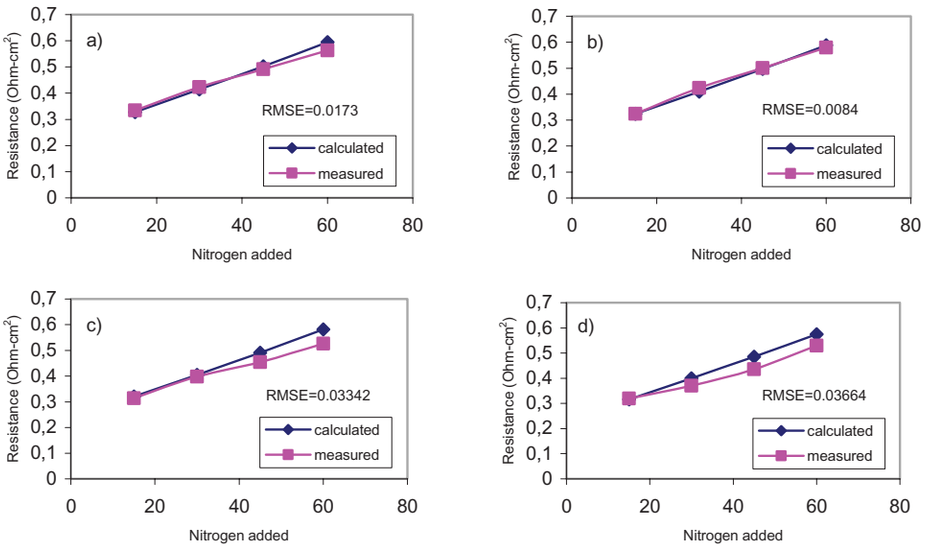

Figure 6. (Color online) Variation of the calculated (R_d) and measured (WR) values of the diffusion resistance for H_2–N_2–H_2O mixtures at various temperatures. At (a) 1173, (b) 1123, (c) 1073, and (d) 1023 K. (Added nitrogen is given as the percentage of the dry mixture which is humidified to 4.2% moisture.)

values (WR) obtained from the fit parameters for Ws for experiments with nitrogen dilution and calculated values (R_d) obtained using Eq. 4.

The experiments with different moisture levels indicated lower diffusion resistance at increasing moisture levels. Figure 7 indicates the calculated and measured values for different moisture levels. Diffusion resistance values obtained from model calculations and from experimental results appear to agree well qualitatively.

Observe from Eq. 4 that variations in the reactant mole fractions and diffusion coefficients cause variations in the calculated values of diffusion resistance. Mole fractions of moisture have a greater influence on the calculated value of the diffusion resistance, because its values are much smaller when compared to the mole fractions of hydrogen. In the experiments with dilution with nitrogen, the mole fraction of moisture in the hydrogen–nitrogen mixture is kept constant while varying the nitrogen mole fraction. For this reason, calculations using hydrogen-moisture binary diffusion coefficients, as used in Eq. 3, do not show comparable variations in the calculated values of diffusion resistance when compared with the experimentally observed values. However, the Stefan–Maxwell diffusion coefficients, $D_{H_2\text{–mix}}$ and $D_{H_2O\text{–mix}}$, show variations on dilution with nitrogen. When the added volume of nitrogen in the mixture increased from 15 to 60% (at constant humidity level of 4.2% and at 1123 K), $D_{H_2O\text{–mix}}$ decreased by 44% and $D_{H_2\text{–mix}}$ decreased by 6%. Variation in $D_{H_2O\text{–mix}}$ compares well with a 44% increase, observed for the diffusion resistance obtained from the measurements (diffusion resistance values from the measurements were obtained when recorded spectra were fitted with the electrical equivalent circuit given in Fig. 3).

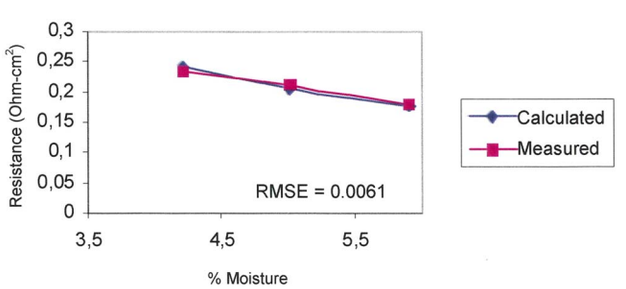

Figure 7. (Color online) Variation in the calculated (R_d) and measured (WR) values of the diffusion resistance, for varying moisture addition at 1123 K.

The rather high value of the diffusion layer thickness is ascribed to the arrangement of the test setup. In the setup, the test cell is in between 5 mm thick ceramic supports, with the test cell placed perpendicular to the direction of the pressure-driven gas flow. This has probably created thick stagnant gas layers on either side of the test cell. Appendix A presents a simplified model of the flow field inside the sample holder generated using the computational fluid dynamics (CFD) software Fluent. It shows the formation of stagnant gas layers on both sides of the test cell. Gas diffusion is mainly from the sides of the sample, thus creating radial concentration gradients inside the reactor (sample holder). The diffusion length is comparable to the radius of the reactor, which is 2 cm. However, in the present case a variety of assumptions is taken for the simplification of the suggested diffusion model, only a qualitative agreement between measured and calculated diffusion resistance values is expected. For this reason, the diffusion layer thickness, assumed for the calculations, probably represents the average thickness of stagnant gas layers on both sides of the test cell. The following factors are expected to cause deviations from the calculations with the simplified assumptions, i.e., (*i*) difference in flow patterns at the bottom and at the top of the sample (due to the structure of the sample holder), (*ii*) reduced area for the fuel flow through the channeled ceramic sample support and the gold meshes, (*iii*) possibility of nonlinear concentration gradients, (*iv*) three-dimensional flow field, (*v*) possible influence of pressure-driven flows, and (*vi*) diffusion of multiple reactants. For a complete quantitative comparison between the measured and calculated values of the diffusion lengths, a significantly more detailed model of the electrochemical reactions combined with the development of detailed CFD models of the gas flow field inside the reactor needs to be developed, which is beyond the scope of this work.

When impedance measurements are carried out on symmetric test cells with Ni/GDC electrodes with gas flows employed as in the present experiments, the obtained results indicate that the gas-phase diffusion process is probably a dominant phenomenon. However, there is a possibility that the pressure-driven flow influences the observed impedance due to the gas-phase diffusion. When this influence is significant, Bessler recently proposed using the name gas concentration impedance for the impedance due to gas-phase processes.[10] To completely understand the extent of this influence, more detailed modeling is required. However, in the present case the simple CFD model shows stagnant gas layers on both sides of the test cell through which diffusion is most probably the dominant mechanism of reactant transport, the measured values of resistance associated with a low frequency arc have very low activation energy,

which is typical for gas-phase diffusion, and the variations in the values of calculated and measured diffusion resistances agree well qualitatively. Hence we consider the observed arc in the low frequency part of the spectra to be due to gas-phase processes, with gas-phase diffusion being the most probable rate-limiting process.

Conclusions

EIS measurements carried out on Ni/GDC electrodes revealed a significant contribution of gas-phase diffusion. The low frequency arc in the spectra originates from diffusion limitations. For H_2, N_2, and H_2O mixtures, a simple model for diffusion resistance using the Stefan–Maxwell diffusion treatment of multicomponent diffusion was suggested. Results from the model calculations agree well qualitatively with experimentally obtained values. The diffusion length computed from the impedance measurement was on the order of centimeters and was higher than reported values. The formation of large gas stagnation zones on both sides of the test cell was considered to be the reason for this large diffusion length. This implies a high level of dependency of the diffusion impedance on gas flow field geometry and reactor design. This in turn implies that a detailed analysis of the test setup and gas flow field is required before evaluation of the impedance spectra obtained on SOFC test cells.

Acknowledgment

P.V. Aravind acknowledges the support and help of Professor H. Spliethoff (TU Munich), N. Woudstra, Z. Qu (TU Delft), and G. Rietveld (ECN) for the work presented in this paper.

Delft University of Technology assisted in meeting the publication costs of this article.

Appendix A
Diffusion Limitation

Here in this work, steady-state gas-phase diffusion is considered across a stagnant gas layer adjacent to the electrodes. On the application of a dc bias, current flow starts and the reacting molecules have to be transported toward the electrodes to sustain the electrochemical reactions at both electrodes as required for the current flow. In the discussion presented here, for simplicity, other electrode responses are omitted by assuming zero charge transfer and other resistances. The following assumptions are made, i.e., (*i*) at very low frequencies, system response to an ac excitation is similar to the one that is due to an applied dc bias, and (*ii*) in that case, one of the electrodes acts as a cathode, liberating oxygen ions from the moisture in the feed gas. These ions then migrate through the electrolyte to the other electrode. Reacting species in the feed gas is transported to the electrodes. Gas diffusion is expected to play a dominant role in this transport. Here, a stagnant layer of thickness l is assumed to be formed over an anode of area A. Diffusion in the stagnant layer proceeds in one dimension and, for simplicity, only a linear gradient in gas concentration across the stagnant layer is considered. Both electrode processes are taken as conservative with respect to the number of gas molecules, and hence pressure-driven diffusion is disregarded. The concentration C_j of electrochemically active species (suffix j = H_2, H_2O, or N_2) at a distance l from the anode surface is equal to that of the bulk gas outside the stagnant layer and is denoted as $C_{j,B}$. The concentration of species at the anode surface (electrode 1) is denoted $C_{j,A}$, and that at the electrode which is acting as the cathode (electrode 2) as $C_{j,C}$ is shown in Fig. A-1. The positive z direction is shown in this figure. The variation in concentration $C_{j,A}$ at the interface is defined as $C_{j,A} - C_{j,B}$ and the variation in concentration $C_{j,C}$ at the interface is defined as $C_{j,C} - C_{j,B}$.

In the dc steady-state case, the diffusion of uncharged species at the anode surface is given by

$$D_{j-mix}\left(\frac{-\Delta C_{j,K}}{\Delta z}\right) = N_j \qquad [A\text{-}1]$$

where N_j is the diffusion flux at the anode surface, D_{j-mix} is the effective diffusion coefficient of species j in a given gas mixture, and $\Delta c_j/\Delta z$ is the concentration gradient of species j at the anode surface. The diffusion flux N_j is controlled by the current density, I, according to the equation

$$N_j = \frac{I}{2F} \qquad [A\text{-}2]$$

For electrode 1

$$\Delta C_{j,A} = C_{j,A} - C_{j,B} \qquad [A\text{-}3]$$

To calculate the effective diffusion coefficient of the gas components in the mixture D_{j-mix}, the Stefan–Maxwell approach for multicomponent diffusion is employed.[15]

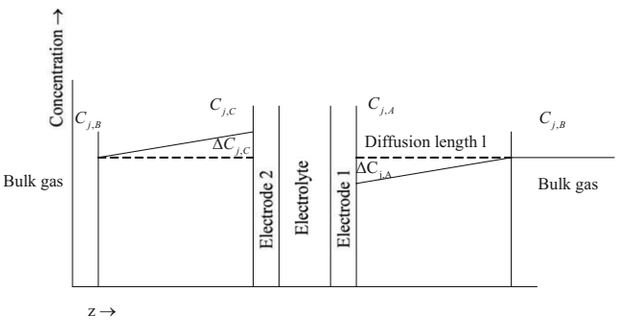

Figure A-1. Gas flow field in the experimental configuration employed.

Now, taking

$$x_j = \frac{C_j}{C} \qquad [A\text{-}4]$$

where x_j is the mole fraction of the jth component and C is the total molar concentration.

Now using the Maxwell equation for multicomponent mixtures and taking D_{i-j} to be the same as Fick's binary diffusion coefficients assuming ideal gas conditions[15]

$$\nabla x_i = \sum_{j-1}^{m} \frac{x_i N_j - x_j N_i}{C D_{i-j}} \qquad [A\text{-}5]$$

Fick's binary diffusion coefficients D_{i-j} in m^2/s for simple molecules can be obtained by applying the Fuller correlation[6]

$$D_{i-j} = \frac{10^{-7} T^{1.75} \sqrt{\frac{1}{M_i} + \frac{1}{M_j}}}{P\left(\sqrt[3]{v_i} + \sqrt[3]{v_j}\right)^2} \qquad [A\text{-}6]$$

where T is the temperature in kelvin, M is the molar weight of the gases, P is the pressure in atmosphere, and v is the diffusion volumes of the species. Here, it is assumed that

$$N_{H_2} = -N_{H_2O} \quad N_{N_2} = 0 \qquad [A\text{-}7]$$

Hence

$$\nabla x_{H_2} = \frac{-N_{H_2}}{C}\left(\frac{x_{H_2}}{D_{H_2-H_2O}} + \frac{x_{H_2O}}{D_{H_2-H_2O}} + \frac{x_{N_2}}{D_{H_2-N_2}}\right) \qquad [A\text{-}8]$$

With the assumption that when $x_j \gg \Delta x_j$, it can be considered that x_j is independent of z and $x_j = x_{j,B}$

$$\nabla x_{H_2} = \frac{dx_{H_2}}{dz} = \frac{\Delta x_{H_2}}{\Delta z} = \frac{-N_{H_2}}{C}\left(\frac{x_{H_2}}{D_{H_2-H_2O}} + \frac{x_{H_2O}}{D_{H_2-H_2O}} + \frac{x_{N_2}}{D_{H_2-N_2}}\right) \qquad [A\text{-}9]$$

$$\frac{\Delta c_{H_2}}{\Delta z} = -N_{H_2}\left(\frac{x_{H_2,b}}{D_{H_2-H_2O}} + \frac{x_{H_2O,b}}{D_{H_2-H_2O}} + \frac{x_{N_2,b}}{D_{H_2-N_2}}\right) \qquad [A\text{-}10]$$

Now D_{H_2-mix} is introduced as

$$D_{H_2-mix}\left(\frac{-\Delta C_{H_2}}{\Delta z}\right) = N_{H_2} \qquad [A\text{-}11]$$

where

$$D_{H_2\ mix} = \frac{1}{\left(\frac{x_{H_2O,B}}{D_{H_2-H_2O}} + \frac{x_{H_2,B}}{D_{H_2-H_2O}} + \frac{x_{N_2,B}}{D_{H_2-N_2}}\right)} \qquad [A\text{-}12]$$

Using a similar approach

$$D_{H_2O-mix}\left(\frac{-\Delta C_{H_2O}}{\Delta z}\right) = N_{H_2O} \qquad [A\text{-}13]$$

$$D_{H_2O-mix} = \frac{1}{\left(\frac{x_{H_2,B}}{D_{H_2-H_2O}} + \frac{x_{H_2O,B}}{D_{H_2-H_2O}} + \frac{x_{N_2,B}}{D_{H_2O-N_2}}\right)} \qquad [A\text{-}14]$$

It can be seen that the same set of equations is valid for electrode 2, and hence the directions of the hydrogen and moisture flows are the same at both electrodes. Now, the open-circuit voltage developed over a complete cell is described in terms of the concentration of oxygen at both anode and cathode, i.e.

$$V = \frac{RT}{4F}\left[\ln\left(\frac{C_{O_2,C}}{C_{O_2,A}}\right)\right] \quad [A\text{-}15]$$

When both electrodes have the H_2, N_2, and H_2O mixtures

$$V = \frac{RT}{2F}\left\{\ln\left[\frac{(C_{H_2O,C}/C_{H_2,C})}{(C_{H_2O,A}/C_{H_2,A})}\right]\right\} \quad [A\text{-}16]$$

Without applied dc bias, the concentrations are the same on both sides and hence the open-circuit voltage is zero. On the application of a dc bias, current flows and this causes a difference in the species concentrations at the electrodes, which is caused by diffusion limitations.

Now, the overpotential due to diffusion is

$$\eta_D = 0 - \frac{RT}{2F}\left[\ln\left(\frac{C_{H_2O,C}}{C_{H_2,C}}\right) - \ln\left(\frac{C_{H_2O,A}}{C_{H_2,A}}\right)\right] \quad [A\text{-}17]$$

$$\eta_D = \frac{RT}{2F}\left[\ln\left(\frac{C_{H_2O,B}}{C_{H_2,B}}\right) - \ln\left(\frac{C_{H_2O,C}}{C_{H_2,C}}\right)\right] - \frac{RT}{2F}\left[\ln\left(\frac{C_{H_2O,B}}{C_{H_2,B}}\right) - \ln\left(\frac{C_{H_2O,A}}{C_{H_2,A}}\right)\right] \quad [A\text{-}18]$$

$$\eta_D = \frac{RT}{2F}\left\{\ln\left[\frac{1 + (\Delta C_{H_2,C}/C_{H_2,B})}{1 + (\Delta C_{H_2O,C}/C_{H_2O,B})}\right]\right\} - \frac{RT}{2F}\left\{\ln\left[\frac{1 + (\Delta C_{H_2,A}/C_{H_2,B})}{1 + (\Delta C_{H_2O,A}/C_{H_2O,B})}\right]\right\} \quad [A\text{-}19]$$

With Taylor expansion $\ln(1 + y) = y$ for $y \ll 1$

$$\eta_D = \frac{RT}{2F}\left[\left(\frac{\Delta C_{H_2,C}}{C_{H_2,B}} - \frac{\Delta C_{H_2O,C}}{C_{H_2O,B}}\right) - \left(\frac{\Delta C_{H_2,A}}{C_{H_2,B}} - \frac{\Delta C_{H_2O,A}}{C_{H_2O,B}}\right)\right] \quad [A\text{-}20]$$

Now from Eq. A-2, it can be seen that

$$\Delta C_{H_2,C} = \frac{Il}{2FD_{H_2\text{–mix}}} \quad [A\text{-}21]$$

$$\Delta C_{H_2O,C} = \frac{-Il}{2FD_{H_2O\text{–mix}}} \quad [A\text{-}22]$$

$$\Delta C_{H_2,A} = \frac{-Il}{2FD_{H_2\text{–mix}}} \quad [A\text{-}23]$$

$$\Delta C_{H_2O,A} = \frac{Il}{2FD_{H_2O\text{–mix}}} \quad [A\text{-}24]$$

Now, from Eq. A-20 and substituting for ΔC values

$$\eta_D = 2\left(\frac{RT}{2F}\right)^2 \frac{l}{P}\left(\frac{1}{D_{H_2O\text{–mix}}X_{H_2O,B}} + \frac{1}{D_{H_2\text{–mix}}X_{H_2,B}}\right)I \quad [A\text{-}25]$$

From Eq. A-2 and A-21-A-25, it can be seen that, for the same applied potential, better performing electrodes and test cells with lower overall impedance cause higher current flows and, in turn, larger differences in concentrations across the stagnant layer. This causes a larger overpotential due to diffusion. But, because the current is also expected to be higher, no significant influence on the diffusion resistance is expected. Hence, it can be assumed that for high performance anodes, the diffusion resistance due to the stagnant gas layer is practically independent of the type of the anode used but mainly depends on the type of the test geometry employed for the measurements and the flow field in it.

Appendix B

Generation of Stagnation-Flow Region on Both Sides of the Electrode

Simplified two-dimensional CFD calculations were carried out to study the gas-flow pattern inside the sample holder near the test cell. The CFD package Fluent was used for the calculations. Humidified hydrogen (with 4.2% moisture) was taken as the flowing fluid at a reactor temperature of 1123 K. Mass and momentum conservation equations were solved. The following settings were employed for the calculations, i.e., (*i*) pressure velocity coupling: simple, (*ii*) pressure discretization: standard, and (*iii*) momentum discretization: second-order upwind. Flow geometry represents the simplified experimental conditions inside the sample holder given in Fig. 1. The reactor diameter was 4 cm and a flow along a 40 cm part of the reactor was modeled. Calculations were carried out with an inlet gas flow of 0.1 N L/min. Gas velocities obtained, shown in Fig. B-1 are given in meters per second. Results indicate the formation of a stagnant zone near the test cell through which gas molecules probably have to diffuse. This stagnant zone probably causes the diffusion impedance.

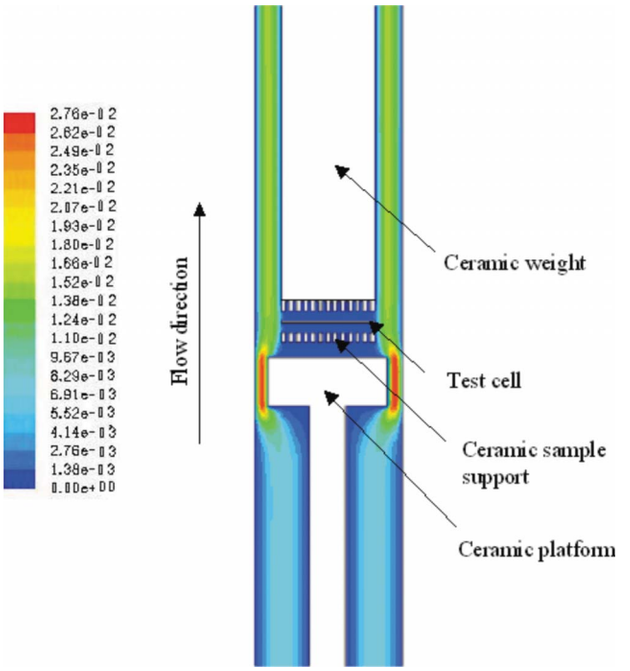

Figure B-1. (Color online) Modeled gas flow through the sample holder.

References

1. P. V. Aravind, Ph.D. Thesis, TU Delft, Delft (2007).
2. P. V. Aravind, J. P. Ouweltjes, N. Woudstra, and G. Rietveld, *Electrochem. Solid-State Lett.*, **11**, B24 (2008).
3. S. Baron, N. Brandon, A. Atkinson, B. Steele, and R. Rudkin, *J. Power Sources*, **126**, 58 (2004).
4. Y. Matsuzaki and I. Yasuda, *Solid State Ionics*, **132**, 261 (2000).
5. J. P. Ouweltjes, P. V. Aravind, N. Woudstra, and G. Rietveld, *J. Fuel Cell Sci. Technol.*, **3**, 495 (2006).
6. S. Primdahl, Ph.D. Thesis, University of Twente and Risø National Laboratory, Twente, Denmark (1999).
7. S. Primdahl and M. Mogensen, *Solid State Ionics*, **152–153**, 597 (2002).
8. A. Weber, B. Sauer, A. C. Müller, D. Herbstritt, and E. Ivers-Tiffée, *Solid State Ionics*, **152–153**, 543 (2002).
9. S. Gewies, W. G. Bessler, V. Sonn, and E. Ivers-Tiffée, *ECS Trans.*, **7**(1), 1573 (2007).
10. W. G. Bessler, *J. Electrochem. Soc.*, **153**, A1492 (2006).
11. W. G. Bessler, *Solid State Ionics*, **176**, 997 (2005).
12. S. Primdahl and M. Mogensen, *J. Electrochem. Soc.*, **145**, 2431 (1998).
13. S. Primdahl and M. Mogensen, *J. Electrochem. Soc.*, **146**, 2827 (1999).
14. J. Ross Macdonald, *Impedance Spectroscopy: Emphasizing Solid Materials and Systems*, John Wiley & Sons, New York (1987).
15. J. A. Wesselingh and R. Krishna, *Mass Transfer in Multicomponent Mixtures*, p. 328, Delft University Press, Delft (2000).